Title:

Homocysteine-induced endoplasmic reticulum stress activates FGF21 via CREBH, resulting in browning and atrophy of white adipose tissue in *Bhmt* knockout mice.

Authors:

Manya Warrier[1], Evan M. Paules[1,3], Walter B. Friday[1], Frances Bramlett[1], Hyunbae Kim[2], Kezhong Zhang [2] and Isis Trujillo-Gonzalez*[1,3]

Affiliations:

[1]Department of Nutrition, UNC Nutrition Research Institute, UNC-Chapel Hill and Kannapolis, NC, USA.

[2] Center for Molecular Medicine and Genetics, Wayne State University School of Medicine, Detroit, MI, USA.

[3] Department of Nutrition, Gillings School of Global Public Health, University of North Carolina at Chapel Hill, Chapel Hill, NC 27514, USA.

Correspondence:

Isis Trujillo-Gonzalez, PhD

Research Assistant Professor

UNC Nutrition Research Institute

University of North Carolina at Chapel Hill

500 Laureate Way, Room 2018

Kannapolis, NC 28081

Email: isis_trujillo@unc.edu

Phone: 704-250-5020

Short title: *Betaine homocysteine S-methyltransferase and lipodisprophy in mice.*

List of abbreviations:

CIDEA	Cell death-inducing DFFA-like effector A
ATF3	Activating Transcription Factor 3
BHMT	Betaine Homocysteine-S-Methyltransferase
BAT	Brown adipose tissue
CHOP	c/EPB homologous protein
CREBH	Cyclic AMP response element binding protein H
FGF21	Fibroblast Growth Factor 21
Hcy	Homocysteine
PCG-α	Peroxisome Proliferator-activated receptor gamma coativator 1-alpha
SAM	S-adenosyl methionine
UCP1	Uncoupling Protein 1
WAT	White adipose tissue

Abstract

Betaine-homocysteine methyltransferase (BHMT) catalyzes the transfer of methyl-groups from betaine to homocysteine (Hcy) producing methionine and dimethylgycine. In this work, we characterize *Bhmt* wildtype (WT) and knockout (KO) mice that were fully backcrossed to a C57Bl6/J background. Consistent with our previous findings, *Bhmt* KO mice had decreased body weight, fat mass and adipose tissue weight compared to WT. Histological analyses and gene expression profiling indicate that adipose browning was activated in KO mice and contributed to the adipose atrophy observed. BHMT is not expressed in adipose tissue but is abundant in liver, thus, a signal must be originating from the liver that modulates adipose tissue. We found that, in Bhmt KO mice, homocysteine-induced endoplasmic reticulum (ER) stress, with activation of hepatic transcription factor cyclin AMP response element binding protein (CREBH), mediated an increase in hepatic and plasma concentrations of fibroblast growth factor 21 (FGF21), which is known to induce adipose browning. CREBH binds to the promoter regions of FGF21 to activate its expression. Taken together, our data indicate that deletion of a single gene in one-carbon metabolism modifies adipose biology and energy metabolism. It would be interesting to determine whether people with functional polymorphisms in *BHMT* exhibit a similar adipose atrophy phenotype.

Keywords

betaine-homocysteine *S*-methyltransferase, lipodystrophy, ER stress, CREBH, BHMT, FGF21, homocysteine

INTRODUCTION

Betaine-homocysteine *S*-methyltransferase (BHMT) is an important Zn-dependent thiol-methyltransferase that catalyzes the formation of methionine from homocysteine using betaine as its methyl donor (1, 2). Methionine is subsequently converted to *S*-adenosylmethionine (SAM) and is used for various methylation reactions (3). BHMT is one of the most abundant proteins in the liver, amounting to 0.6-1% of total protein (4), and it is also found in kidney, the eye lens, and at lower activities in other tissues, but not in adipose (5, 6). Mice in which *Bhmt* was deleted (whole body; *Bhmt* KO) have increased hepatic concentrations of the substrates betaine and homocysteine (Hcy) (5, 7). These KO mice develop increased energy expenditure associated with lower body weight compared to their wild type (WT) littermates and develop lipodystrophy and fatty liver (5, 7). At 1 year of age, 64% of *Bhmt* KO mice develop hepatic tumors (5, 7). Though the mechanisms underlying the hepatocarcinogenesis have been explored (3), those involved in the adipose wasting have not been addressed, we do so in this paper.

In this study, we show that deletion of *Bhmt* in mice causes increased Hcy concentrations in tissues, and that this initiates a signaling cascade involving endoplasmic reticulum stress (ER stress) with activation (cleavage) of cyclic AMP response element binding protein H (CREBH) generating a transcription factor that promotes the expression of genes including fibroblast growth factor 21 (*Fgf21*; previously, we reported increased Fgf21 concentrations produced by the liver in *Bhmt* KO mice (7)). Fgf21 stimulates adipose browning and energy expenditure by upregulating the expression of the transcriptional co-activator peroxisome proliferator-activated receptor gamma coactivator **1**-alpha (Pgc-1α), as well as uncoupling protein 1 (Ucp1). This culminates in adipose wasting in *Bhmt* KO mice.

Results

Deletion of Bhmt promotes adipose atrophy in fully backcrossed mice

We previously reported that *Bhmt* knockout mice on a mixed 129/SV x C57BL/6J background (generations F3-F5), between 7-12 weeks of age, had reduced adipose mass and smaller-sized adipocytes (7). Since genetic background of mice can have a profound influence on the metabolic phenotype of mice (8), we decided to reexamine this lipodystrophy phenotype after backcrossing *Bhmt* KO mice to C57Bl/6 to generate a near congenic (99.74%) line. In this near congenic line, we confirmed that, in the *Bhmt* KO compared to wild type (WT), there was a significant reduction in total body weight (**Fig 1A**) and adipose weight **(Fig 1B)** in mice. Histological analysis of adipose tissue taken from *Bhmt* KO mice showed reduced adipocyte cell size and reduced size of lipid droplets in both gonadal white adipose tissue (gWAT; data not shown) and inguinal white adipose tissue (iWAT) as compared to WT **(Fig 1C and Fig 1D)**. Adipose atrophy is characterized by reduced fat/lean mass and the 'slimming of adipocytes' in both size and volume (9), and our data show that this process was dependent on *Bhmt* status.

Adipose atrophy in Bhmt KO *mice is associated with adipose browning in inguinal adipose depots*

Since smaller adipocytes and increased whole body energy expenditure and heat production are classical features of browning of WAT (10), and since adipose browning is known to promote adipose atrophy in several mouse models (10-14), we sought to determine whether the WAT atrophy observed in *Bhmt* KO mice is due to WAT browning. We first measured a number of molecular markers that are frequently associated with adipose browning (15-17). Uncoupling Protein 1 (*Ucp1)* mRNA **(Fig 2A)** along with mRNA for other thermogenic genes such as Peroxisome proliferator-activated receptor gamma coactivator 1-alpha (*Pgc-1α)* and the lipid-droplet-associated protein cell death-inducing DFFA-like effector A (*CideA*) **(Fig 2B – C)** were all

126 significantly upregulated in iWAT collected from *Bhmt* KO mice compared to WT. Together, these
127 results indicate that lack of *Bhmt* is sufficient to induce the expression of adipose browning
128 markers.
129
130 ***Bhmt* KO *livers have increased homocysteine concentrations***
131 Plasma total Hcy concentrations were significantly increased in *Bhmt* KO mice on a mixed 129/SV
132 x C57BL/6J background (generations F3-F5), as we previously reported (7). We now show that,
133 in the fully backcrossed *Bhmt* KO mice, both plasma Hcy concentrations (~11 fold) and liver Hcy
134 concentrations (~2 fold) were increased in KO as compared to WT mice (**Fig 3A and B**). Thus,
135 loss of *Bhmt* results in the accumulation of plasma and liver Hcy .
136
137 ***Bhmt* KO *livers have increased ER stress and have more activated CREBH***
138 Since high tissue Hcy is a known cause of ER stress, which in turn regulates a number of
139 transcription factors residing in the ER (18, 19), we decided to see if *Bhmt* KO mice experience
140 increased ER stress compared to WT. We measured gene expression of DNA damage-inducible
141 transcript 3, also known as C/EBP homologous protein (CHOP) and Activating Transcription
142 Factor 3 (ATF3), as indicators of ER stress (20-30). We found that expression of these genes
143 were increased by 1.5-fold and 3-fold, respectively, in *Bhmt* KO compared to WT mouse livers
144 (**Figs 4A and 4B**). Thus, *Bhmt* KO mice have increased ER stress compared to their WT
145 counterparts.
146
147 Next, we searched for transcription factors that reside in the ER and are produced in response to
148 ER stress and which are also known to regulate FGF21. We found that the hepatic transcription
149 factor known as Cyclin AMP Responsive Element Binding Protein – H (CREBH) fulfilled the above
150 criteria (19, 31, 32). We measured full length and activated CREBH in the liver lysates prepared

from both *Bhmt* WT and KO mice by Western blot analysis and found that the cleaved activated form of CREBH was significantly increased in *Bhmt* KO compared to WT liver **(Figs 4C and 4D**).

Bhmt* KO *livers have increased FGF21 concentrations

Since activated CREBH binds to the *Fgf21* promoter and activates its transcription (33), we suggest that this explains our earlier finding that *Bhmt* KO mice on a mixed 129/SV x C57BL/6J background (generations F3-F5) had increased FGF21 concentrations (7). We now show that in fully backcrossed *Bhmt* KO mice, compared to WT, plasma and hepatic FGF21 concentrations were increased more than 2-fold (**Figs 5A and 5B**).

Discussion

The deletion of *Bhmt* in mice results in the animal storing less fat in adipose tissue even though BHMT is not expressed in adipose tissue (7). This adipose atrophy is the result of reduced triglyceride storage within iWAT associated with increased energy expenditure and heat production as measured by indirect colorimetry without a matching increase in food consumption (7). We now report that the elevated Hcy concentrations that occur when the *Bhmt* gene is deleted, increase ER stress signalling, which results in generation of activated CREBH, and this, in turn, caused increased expression in hepatic FGF21. This FGF21 is transported via blood to adipocytes where it promotes the browning of white adipose tissue and increases expression of PGC-1α which increases mitochondrial number, and increases the expression of UCP-1 which uncouples mitochondrial respiration and thereby increases energy expenditure and heat production. (**Fig 6**).

As noted earlier, BHMT catalyzes the formation of methionine from Hcy using betaine as its methyl donor (1, 2). As expected, deletion of *Bhmt* should increase concentrations of both substrates (betaine and Hcy) used by this enzyme. Increased concentrations of Hcy cause ER stress both

177 *in vitro* and *in vivo* (20, 21, 23, 26, 27, 30, 34-36) by disrupting disulfide bond formation and thus
178 leading to protein misfolding (21). Though we argue that it is the the accumulation of Hcy that
179 results in ER stress and subsequent browning of adipose tissue, it is possible that the
180 accumulation of the other precursor, betaine, also contributes to adipocyte browning as feeding
181 mice a diet containing 5% betaine increases plasma concentrations of FGF21 (7, 37). Since *Bhmt*
182 deletion resulted in reduced methylation potential by increasing *S*-adenosylhomocysteine
183 concentrations, in earlier studies we examined whether the FGF21 promoter region might be
184 hypomethylated in the *Bhmt* KO mouse, leading to increased expression of this gene. However,
185 reduced representation bisulfite sequencing performed on liver DNA from WT and KO mice did
186 not reveal any methylation differences in this gene (3).
187
188 ER stress is initiated by numerous metabolic stressors including high concentrations of
189 homocysteine (20, 21, 23, 26) and has been associated with hepatic lipid accumulation, obesity
190 and cancer (24, 38). Also, it has been implicated in WAT browning (39). Transcription factors that
191 are regulated by ER stress include Sterol Regulatory Element Binding Proteins (SREBP) and
192 CREBH (29). CREBH is ER-tethered and is synthesized in the liver as a precursor which then
193 gets activated via cleavage by Golgi-localized proteases and the activated form then accumulates
194 in the nucleus to act as a transcription factor (19) that promotes expression of the liver-secreted
195 peptide endocrine hormone FGF21 (31, 33). Promoter analysis studies show that CREBH can
196 bind and activate FGF21 promoter at position -60 to -40 bp. Chromatin immunoprecipitation
197 studies reveal that CREBH directly binds to the FGF21 promoter and controls the expression and
198 plasma levels of FGF21 (33, 40). Using CREBH KO and CREBH over-expression mouse models
199 it has been shown that FGF21 mediates many of CREBH's effects on fatty acid metabolism and
200 ketogenesis (41). Also, FGF21 is responsible for the body weight loss induced by CREBH over-
201 expression and particularly the fat mass reduction (31). Therefore, it is reasonable to propose that
202 CREBH is the upstream transcriptional regulator of FGF21 in *Bhmt* KO mice. In addition to

deletion of *Bhmt*, essential amino acid restriction, fasting and impaired muscular and hepatic autophagy induce ER stress and result in substantial increases in circulating FGF21 and UCP1 levels in adipose (42, 43).

Many endocrine and autocrine signals stimulate adipose browning, including FGF21 (44). FGF21 binds to its receptor (FGFR) and coreceptor β-Klotho (KLB) to activate a downstream signaling cascade that ultimately leads to expression of its target genes (43). FGF21 stimulates adipose browning and energy expenditure by upregulating the expression of transcriptional co-activator PGC-1α in adipose tissue (17, 43, 45). Browning of white adipose tissue is characterized by the appearance of brown-like or beige adipocytes within WAT (46, 47). These inducible beige adipocytes are morphologically similar to brown adipocytes and express uncoupling protein 1 and contribute to thermogenesis (39, 47).

As noted earlier, adipose atrophy is characterized by reduced fat/lean mass and the excessive 'slimming of adipocytes' in both size and volume (9). Increased metabolic rate and adipose browning has been proposed as causes for adipose atrophy (9, 11-14, 48-52). Even though browning of WAT is generally considered beneficial in obesity (reducing body weight and increasing energy expenditure), several lines of evidence suggest that it also is associated with adverse outcomes such as hepatic steatosis, cancer associated cachexia (CAC) and burn-related cachexia (11, 14, 49, 50).

Is reduced BHMT expression likely to be a problem in people? Several functional *Bhmt* variants have been identified in humans which are associated with increased risk for cancer and other diseases (53-56), however no information is available on the metabolic phenotype of humans carrying those variants. It would be interesting to explore whether people with functional *Bhmt* variants have a metabolic phenotype similar to that which we describe in mice, and determine

whether proposed Hcy-CREBH-FGF21–adipose browning pathway drives this phenotype. This would not only help us to understand how genetic variations in one carbon metabolism affect obesity but also our understanding of how adipose atrophy develops in diseases such as cancer.

MATERIALS AND METHODS

Animals. Mice used in these experiments were bred and maintained at the David H. Murdock Research Institute (DHMRI), Center for Laboratory Animal Science facilities. All animal experiments were performed in accordance with the protocols approved by David H. Murdock Research Institute Institutional Animal Care and Use Committee. The study was carried out in compliance with the ARRIVE guidelines.

Bhmt KO mice were generated as previously described (5). *Bhmt* KO mice were fully backcrossed to C57B1/6 wild-type mice to generate a near congenic (99.73 %) mouse line. Genotyping of *Bhmt* animals was performed using the following primers: *Bhmt* WT_F 5'–GACTTT TAAAGAGTGGTGGTACATACCTTG-3', *Bhmt* WT_R -5' –TCTCTCTGCAGCCACATCTGAACTTGTCTG-3', *Bhmt* KO_F- 5' –TTAACTCAACATCACAACAACAGATTTCAG -3', *Bhmt* KO_R 5' –TTG TCGACGGATCCATAACTTCGTATAAT -3'. *Bhmt* WT and KO mice were mated and maintained *ad libitum* on a AIN 76A diet (Dyets, Bethelehem, PA, USA) and were kept in a temperature-controlled environment at 24°C and exposed to a 12 hours light and dark cycle. At 6-8 weeks, mice were euthanized and tissue collection was performed.

Histological analysis. Tissues were fixed in buffered formalin, dehydrated in ethanol and then transferred to xylene solution for embedding in paraffin. Serial sections at 5 mm thickness were made from paraffin-embedded tissue and then stained with hematoxylin and eosin. Images were analyzed with light microscopy. Adipocyte area was calculated by measuring the area of cells per condition, at 200x magnification, using Image J, and presented as mean ± SEM.

RT-PCR analysis. Total RNA was extracted from tissues of *Bhmt* WT and *Bhmt* KO mice, using RNAeasy mini Kit (Qiagen, Hilden, Germany). cDNA synthesis was performed by using a Script™ cDNA SuperMix (Quanta BioSciences, Gaithrsburg, MD, USA). For quantitative real-time assays, amplification was performed by using PerfeCTa qPCR FastMix (Quanta Biosciences). We designed primers (Sigma) as follows: ***UCP1*** forward primer: ACTGCCACAACCTCCAGTCATT, reverse primer CTTTGCCTCACTCAGGATTGG; **PGC1a** forward primer AGCCGTGACCACTGACAACGAG, reverse primer GCTGCATGGTTCTGAGTGCTAGG; ***CIDEA*** forward primer: GCAACCAAAGAAATGCGGAATAG, reverse primer: CTCGTACATCGTGGCTTTGA; ***CHOP*** forward primer CAGCGACAGAGCCAGAAT; ***ATF3*** forward primer GAGGCGGCGAGAAAGAAA, reverse primer CACACTCTCCAGTTTCTC. Ct values were calculated by SDS 1.2 software (Applied Biosystems, Foster City, CA, USA) and normalized to *TATA* binding Ct values and expressed as $2^{-(Ct(gene)- Ct (housekeeping\ gene))}$.

Western blot. Liver tissues were collected to evaluate CREBH levels. Protein extracts were preparared using RIPA lysis buffer (Sigma, ST. Louis, USA) supplemented with protease inhibitor cocktail (Complete, Roche) and sonicated. Total protein concentrations for all samples was quantified using BCA protein assay (Bio-Rad, Hercules, CA, USA). Proteins were loaded into SDS-PAGE gels and blotted on PVDF membranes. CREBH antibody was used at 1:1000 dilution. Enhancer chemiluminescence was used to detect protein. CREBH protein abundance was quantified using Image J (NIH, Bethesda, MD, USA). Data are presented mean ± SEM.

FGF21 measurement.

Serum: Blood samples from *Bhmt* WT and *Bhmt* KO mice, were collected and were subjected to centrifugation at 1000 g for 15 min at 4°C. **Liver**: Crushed liver samples were homogenized in cold phosphate-buffered saline (PBS) (Sigma) with protease inhibitors (Roche). Samples were

subjected to centrifugation at 9,600 g for 15 minutes at 4° C. For both plasma and liver, supernantatant protein was quantified using BCA protein assay (Bio-Rad, Hercules, CA, USA) and diluted to equal concentrations before performing an enzyme-linked immunoabsorbent assay (ELISA) using a Mouse/Rat FGF21 Quantikine ELISA kit (R&D Systems, Minneapolis, MN)(57) .

Homocysteine measurement. Plasma or liver was homogenized in dithiothreitol (DTT) and processed to dissociate the proteins by filtration, thereby extracting protein-bound Hcy. The protein-free filtrate was analyzed for total Hcy by liquid chromatography-electrospray ionization-tandem mass spectrometry (LC-ESI-MS/MS) as previously described (58, 59).

Statistical analysis. The number of samples per group are indicated in the figure legends. There were no experimental units or data points excluded. Statistical analyses were performed with Prism 7 (GraphPad Software, La Jolla, CA, USA). Data distribution was tested for statistical normality. The Brown-Forsythe test (F test) was used to compare group variances. Groups with equal distribution were compared using Students' t test. Groups with unequal variances were compared using the nonparamentric Mann-Whitney test. Data are presented as means ± SEM.

Acknowledgments.

The authors thank Jennifer Owen (University of North Carolina at Chapel Hill, Nutrition Research Institute) for providing assistance with experiments; Dr. Steve Orena (University of North Carolina at Chapel Hill, Nutrition Research Institute) for providing metabolite services. This work was supported by U.S National Institutes of Health (NIH), National Institute of Diabetes and Digestive and Kidney Diseases Grants DK056350 and DK115380 (To Dr. Steven Zeisel).

Author contributions.

M. W. performed experiments, analyzed the data, conceived the study and wrote the manuscript, E. M. P. performed experiments, W. B. F. performed experiments, F.B. performed experiments, H. K. performed western blot experiments, K. Z. performed experiments, I. T-G. developed study designs, performed experiments, analyzed and interpreted the data, prepared figures and wrote the manuscript.

Competing interests.

The authors declare no competing interests.

FIGURE LEGENDS.

FIGURE 1. Lack of the *Bhmt* gene induces adipose atrophy in mice. (A) Bodyweight loss of Bhmt knockout (*Bhmt-KO*) compared to Bhmt wild type (*Bhmt-WT).* **(B)** Adipose weight normalized over body weight. *n*= 25 *Bhmt-KO; n*= 24 *Bhmt-WT*. **(C) and (D)** Representative stainings of sections from inguinal white adipose tissue (iWAT) from *Bhmt-WT* **(C)** and *Bhmt-KO* **(D)** Scale bar= 50 mm. Results represent mean ± SEM. ****P≤0.0001 by unpaired t-test.

FIGURE 2. Lack of the *Bhmt* gene induces the expression of beige remodeling markers that induce browning. mRNA levels of beige remodeling markers *Ucp1* **(A),** *Pgc1a* **(B),** and *Cidea* **(C)** in inguinal adipose tissue (iWAT) of *Bhmt-WT* and *Bhmt-KO* mice. Relative quantitative values (normalized to 36B4) are reported as fold change. Results represent mean ± SEM. *P≤0.05, **P≤0.01 by Mann-Whitney test (A and C) and by unpaired t-test (B and D). *n* = 10 per group.

FIGURE 3. Increase in plasma and liver homocysteine (Hcy) levels in *Bhmt-KO* mice. (A) Plasma levels of Hcy are increased in *Bhmt-KO* mice ~50 fold when compared with *Bhmt-WT* mice. *n*=5 per group. **(B)** Liver Hcy levels were also increased ~20 fold in *Bhmt-KO* mice when compared with *Bhmt-WT. n*= 7 *Bhmt-KO; n*=5 *Bhmt-WT.* Results represent mean ± SEM. *P≤0.05, **P≤0.01 by Mann-Whitney test.

FIGURE 4. Endoplasmic reticulum (ER) stress is increased in *Bhmt-KO* livers and exhibit activation of CREBH. mRNA levels of ER stress markers *Chop* **(A)** *n*= 10 per group, and *Atf3* **(B)** are increased in liver *Bhmt-KO* mice compared to WT. *n*= 7 *Bhmt-KO; n*=8 *Bhmt-WT* Relative quantitative values (normalized to 36B4) are reported as fold change. Results represent mean ± SEM. *P≤0.05, **P≤0.01 by unpaired t-test (A) and Mann Whitney test (B). **(C)** Representative western blot of full-length CREBH and cleaved CREBH from *Bhmt-*

WT and *Bhmt-KO*. GAPDH was used as a loading control. **(D)** The ratio of cleavaged CREBH divided by full-length CREBH. *P≤0.05 by unpaired t-test.

FIGURE 5. FGF21 is increased in *Bhmt-KO* plasma and liver. (A) Plasma FGF21 levels are increased in plasma from *Bhmt-KO* mice when compared to *Bhmt-WT. n*=9 per group Results represent mean ± SEM. *P≤0.05 by *t*-test. **(B)** mRNA levels of Fgf21 in the liver are increased ~2 fold. Relative quantitative values (normalized to 36B4) are reported as fold change. ****P≤0.0001 by *t*-test. *n*=5 per group.

FIGURE 6. Schematic representation of the effects of the deletion of *Bhmt* in liver and iWAT. The schema summarizes our new findings where deletion of *Bhmt* in mice increases homocysteine levels leading to endoplasmic reticulum (ER) stress. ER stress led to an increase in the cleaved CREBH protein levels, which acts as a transcription factor that binds the FGF21 promoter**.** FGF21 high levels exert their effects in iWAT.

References

1. Abdelmalek MF, Angulo P, Jorgensen RA, Sylvestre PB, Lindor KD. Betaine, a promising new agent for patients with nonalcoholic steatohepatitis: results of a pilot study. Am J Gastroenterol. 2001;96(9):2711-7.
2. Zhang K, Shen X, Wu J, Sakaki K, Saunders T, Rutkowski DT, et al. Endoplasmic reticulum stress activates cleavage of CREBH to induce a systemic inflammatory response Role of Endoplasmic Reticulum Stress and Unfolded Protein Responses in Health and Diseases. Cell. 2006;124(3):587-99.
3. Lupu DS, Orozco LD, Wang Y, Cullen JM, Pellegrini M, Zeisel SH. Altered methylation of specific DNA loci in the liver of Bhmt-null mice results in repression of Iqgap2 and F2rl2 and is associated with development of preneoplastic foci. FASEB journal : official publication of the Federation of American Societies for Experimental Biology. 2017;31(5):2090-103.
4. Pajares MA, Perez-Sala D. Betaine homocysteine S-methyltransferase: just a regulator of homocysteine metabolism? Cell Mol Life Sci. 2006;63(23):2792-803.
5. Teng YW, Mehedint MG, Garrow TA, Zeisel SH. Deletion of betaine-homocysteine S-methyltransferase in mice perturbs choline and 1-carbon metabolism, resulting in fatty liver and hepatocellular carcinomas. J Biol Chem. 2011;286(42):36258-67.
6. Ganu RS, Garrow TA, Sodhi M, Rund LA, Schook LB. Molecular characterization and analysis of the porcine betaine homocysteine methyltransferase and betaine homocysteine methyltransferase-2 genes. Gene. 2011;473(2):133-8.
7. Teng YW, Ellis JM, Coleman RA, Zeisel SH. Mouse betaine-homocysteine S-methyltransferase deficiency reduces body fat via increasing energy expenditure and impairing lipid synthesis and enhancing glucose oxidation in white adipose tissue. J Biol Chem. 2012;287(20):16187-98.
8. Stockli J, Fisher-Wellman KH, Chaudhuri R, Zeng XY, Fazakerley DJ, Meoli CC, et al. Metabolomic analysis of insulin resistance across different mouse strains and diets. J Biol Chem. 2017;292(47):19135-45.
9. Bing C, Trayhurn P. New insights into adipose tissue atrophy in cancer cachexia. Proc Nutr Soc. 2009;68(4):385-92.
10. Peschechera A, Eckel J. "Browning" of adipose tissue--regulation and therapeutic perspectives. Arch Physiol Biochem. 2013;119(4):151-60.
11. Petruzzelli M, Wagner EF. Mechanisms of metabolic dysfunction in cancer-associated cachexia. Genes Dev. 2016;30(5):489-501.
12. Han J, Meng Q, Shen L, Wu G. Interleukin-6 induces fat loss in cancer cachexia by promoting white adipose tissue lipolysis and browning. Lipids Health Dis. 2018;17(1):14.
13. Kir S, Komaba H, Garcia AP, Economopoulos KP, Liu W, Lanske B, et al. PTH/PTHrP Receptor Mediates Cachexia in Models of Kidney Failure and Cancer. Cell Metab. 2016;23(2):315-23.
14. Petruzzelli M, Schweiger M, Schreiber R, Campos-Olivas R, Tsoli M, Allen J, et al. A switch from white to brown fat increases energy expenditure in cancer-associated cachexia. Cell Metab. 2014;20(3):433-47.
15. Ohno H, Shinoda K, Ohyama K, Sharp LZ, Kajimura S. EHMT1 controls brown adipose cell fate and thermogenesis through the PRDM16 complex. Nature. 2013;504(7478):163-7.
16. Defour M, Dijk W, Ruppert P, Nascimento EBM, Schrauwen P, Kersten S. The Peroxisome Proliferator-Activated Receptor alpha is dispensable for cold-induced adipose tissue browning in mice. Mol Metab. 2018;10:39-54.

17. Fisher FM, Kleiner S, Douris N, Fox EC, Mepani RJ, Verdeguer F, et al. FGF21 regulates PGC-1alpha and browning of white adipose tissues in adaptive thermogenesis. Genes Dev. 2012;26(3):271-81.
18. Colgan SM, Hashimi AA, Austin RC. Endoplasmic reticulum stress and lipid dysregulation. Expert Rev Mol Med. 2011;13:e4.
19. Wang M, Zhao S, Tan M. bZIP transmembrane transcription factor CREBH: Potential role in non-alcoholic fatty liver disease (Review). Mol Med Rep. 2016;13(2):1455-62.
20. Ai Y, Sun Z, Peng C, Liu L, Xiao X, Li J. Homocysteine Induces Hepatic Steatosis Involving ER Stress Response in High Methionine Diet-Fed Mice. Nutrients. 2017;9(4).
21. Dionisio N, Jardin I, Salido GM, Rosado JA. Homocysteine, intracellular signaling and thrombotic disorders. Curr Med Chem. 2010;17(27):3109-19.
22. Faust PL, Kovacs WJ. Cholesterol biosynthesis and ER stress in peroxisome deficiency. Biochimie. 2014;98:75-85.
23. Kaplowitz N, Than TA, Shinohara M, Ji C. Endoplasmic reticulum stress and liver injury. Semin Liver Dis. 2007;27(4):367-77.
24. Lebeaupin C, Vallee D, Hazari Y, Hetz C, Chevet E, Bailly-Maitre B. Endoplasmic Reticulum stress signaling and the pathogenesis of Non-Alcoholic Fatty Liver Disease. J Hepatol. 2018.
25. Mahdi AA, Rizvi SH, Parveen A. Role of Endoplasmic Reticulum Stress and Unfolded Protein Responses in Health and Diseases. Indian J Clin Biochem. 2016;31(2):127-37.
26. Wang CY, Zou W, Liang XY, Jiang ZS, Li X, Wei HJ, et al. Hydrogen sulfide prevents homocysteineinduced endoplasmic reticulum stress in PC12 cells by upregulating SIRT1. Mol Med Rep. 2017;16(3):3587-93.
27. Werstuck GH, Lentz SR, Dayal S, Hossain GS, Sood SK, Shi YY, et al. Homocysteine-induced endoplasmic reticulum stress causes dysregulation of the cholesterol and triglyceride biosynthetic pathways. J Clin Invest. 2001;107(10):1263-73.
28. Zhang C, Chen X, Zhu RM, Zhang Y, Yu T, Wang H, et al. Endoplasmic reticulum stress is involved in hepatic SREBP-1c activation and lipid accumulation in fructose-fed mice. Toxicol Lett. 2012;212(3):229-40.
29. Zhang K, Shen X, Wu J, Sakaki K, Saunders T, Rutkowski DT, et al. Endoplasmic reticulum stress activates cleavage of CREBH to induce a systemic inflammatory response. Cell. 2006;124(3):587-99.
30. Zhang Z, Wei C, Zhou Y, Yan T, Wang Z, Li W, et al. Homocysteine Induces Apoptosis of Human Umbilical Vein Endothelial Cells via Mitochondrial Dysfunction and Endoplasmic Reticulum Stress. Oxid Med Cell Longev. 2017;2017:5736506.
31. Nakagawa Y, Satoh A, Yabe S, Furusawa M, Tokushige N, Tezuka H, et al. Hepatic CREB3L3 controls whole-body energy homeostasis and improves obesity and diabetes. Endocrinology. 2014;155(12):4706-19.
32. Park JG, Xu X, Cho S, Hur KY, Lee MS, Kersten S, et al. CREBH-FGF21 axis improves hepatic steatosis by suppressing adipose tissue lipolysis. Sci Rep. 2016;6:27938.
33. Kim H, Mendez R, Zheng Z, Chang L, Cai J, Zhang R, et al. Liver-enriched transcription factor CREBH interacts with peroxisome proliferator-activated receptor alpha to regulate metabolic hormone FGF21. Endocrinology. 2014;155(3):769-82.
34. Outinen PA, Sood SK, Liaw PC, Sarge KD, Maeda N, Hirsh J, et al. Characterization of the stress-inducing effects of homocysteine. Biochem J. 1998;332 (Pt 1):213-21.

35. Outinen PA, Sood SK, Pfeifer SI, Pamidi S, Podor TJ, Li J, et al. Homocysteine-induced endoplasmic reticulum stress and growth arrest leads to specific changes in gene expression in human vascular endothelial cells. Blood. 1999;94(3):959-67.
36. Curro M, Condello S, Caccamo D, Ferlazzo N, Parisi G, Ientile R. Homocysteine-induced toxicity increases TG2 expression in Neuro2a cells. Amino Acids. 2009;36(4):725-30.
37. Ejaz A, Martinez-Guino L, Goldfine AB, Ribas-Aulinas F, De Nigris V, Ribo S, et al. Dietary Betaine Supplementation Increases Fgf21 Levels to Improve Glucose Homeostasis and Reduce Hepatic Lipid Accumulation in Mice. Diabetes. 2016;65(4):902-12.
38. Oakes SA, Papa FR. The role of endoplasmic reticulum stress in human pathology. Annu Rev Pathol. 2015;10:173-94.
39. Abdullahi A, Jeschke MG. White Adipose Tissue Browning: A Double-edged Sword. Trends Endocrinol Metab. 2016;27(8):542-52.
40. Nakagawa Y, Satoh A, Yabe S, Furusawa M, Tokushige N, Tezuka H, et al. Hepatic CREB3L3 controls whole-body energy homeostasis and improves obesity and diabetes
CREB3L3 controls fatty acid oxidation and ketogenesis in synergy with PPARalpha. Endocrinology. 2014;155(12):4706-19.
41. Nakagawa Y, Satoh A, Tezuka H, Han SI, Takei K, Iwasaki H, et al. CREB3L3 controls fatty acid oxidation and ketogenesis in synergy with PPARalpha. Sci Rep. 2016;6:39182.
42. Fisher FM, Maratos-Flier E. Understanding the Physiology of FGF21. Annu Rev Physiol. 2016;78:223-41.
43. Itoh N. FGF21 as a Hepatokine, Adipokine, and Myokine in Metabolism and Diseases. Front Endocrinol (Lausanne). 2014;5:107.
44. Hu J, Christian M. Hormonal factors in the control of the browning of white adipose tissue. Horm Mol Biol Clin Investig. 2017;31(1).
45. Potthoff MJ, Inagaki T, Satapati S, Ding X, He T, Goetz R, et al. FGF21 induces PGC-1alpha and regulates carbohydrate and fatty acid metabolism during the adaptive starvation response. Proc Natl Acad Sci U S A. 2009;106(26):10853-8.
46. Sepa-Kishi DM, Ceddia RB. White and beige adipocytes: are they metabolically distinct? Horm Mol Biol Clin Investig. 2018;33(2).
47. Sepa-Kishi DM, Ceddia RB, Jankovic A, Otasevic V, Stancic A, Buzadzic B, et al. White and beige adipocytes: are they metabolically distinct?
Physiological regulation and metabolic role of browning in white adipose tissue. Horm Mol Biol Clin Investig. 2018;33(2).
48. Vaitkus JA, Celi FS. The role of adipose tissue in cancer-associated cachexia. Exp Biol Med (Maywood). 2017;242(5):473-81.
49. Argiles JM, Busquets S, Stemmler B, Lopez-Soriano FJ. Cancer cachexia: understanding the molecular basis. Nat Rev Cancer. 2014;14(11):754-62.
50. Kir S, Spiegelman BM. CACHEXIA & BROWN FAT: A BURNING ISSUE IN CANCER. Trends Cancer. 2016;2(9):461-3.
51. Kulyte A, Lorente-Cebrian S, Gao H, Mejhert N, Agustsson T, Arner P, et al. MicroRNA profiling links miR-378 to enhanced adipocyte lipolysis in human cancer cachexia. Am J Physiol Endocrinol Metab. 2014;306(3):E267-74.
52. Vegiopoulos A, Rohm M, Herzig S. Adipose tissue: between the extremes. EMBO J. 2017;36(14):1999-2017.

519 53. Pellanda H, Namour F, Fofou-Caillierez M, Bressenot A, Alberto JM, Chery C, et al. A
520 splicing variant leads to complete loss of function of betaine-homocysteine methyltransferase
521 (BHMT) gene in hepatocellular carcinoma. Int J Biochem Cell Biol. 2012;44(2):385-92.
522 54. Gibson TM, Brennan P, Han S, Karami S, Zaridze D, Janout V, et al. Comprehensive
523 evaluation of one-carbon metabolism pathway gene variants and renal cell cancer risk. PLoS One.
524 2011;6(10):e26165.
525 55. Feng Q, Kalari K, Fridley BL, Jenkins G, Ji Y, Abo R, et al. Betaine-homocysteine
526 methyltransferase: human liver genotype-phenotype correlation. Mol Genet Metab.
527 2011;102(2):126-33.
528 56. Li F, Feng Q, Lee C, Wang S, Pelleymounter LL, Moon I, et al. Human betaine-
529 homocysteine methyltransferase (BHMT) and BHMT2: common gene sequence variation and
530 functional characterization. Mol Genet Metab. 2008;94(3):326-35.
531 57. Archer A, Venteclef N, Mode A, Pedrelli M, Gabbi C, Clément K, et al. Fasting-induced
532 FGF21 is repressed by LXR activation via recruitment of an HDAC3 corepressor complex in mice.
533 Molecular Endocrinology. 2012;26(12):1980-90.
534 58. Lai S-C, Nakayama Y, Sequeira JM, Wlodarczyk BJ, Cabrera RM, Finnell RH, et al. The
535 transcobalamin receptor knockout mouse: a model for vitamin B12 deficiency in the central
536 nervous system. FASEB J. 2013;27(6):2468-75.
537 59. Ducros V, Belva-Besnet H, Casetta B, Favier A. A robust liquid chromatography tandem
538 mass spectrometry method for total plasma homocysteine determination in clinical practice. Clin
539 Chem Lab Med. 2006;44(8):987-90.
540

541

542

543

544

545

546

547

548

549

Figure 1

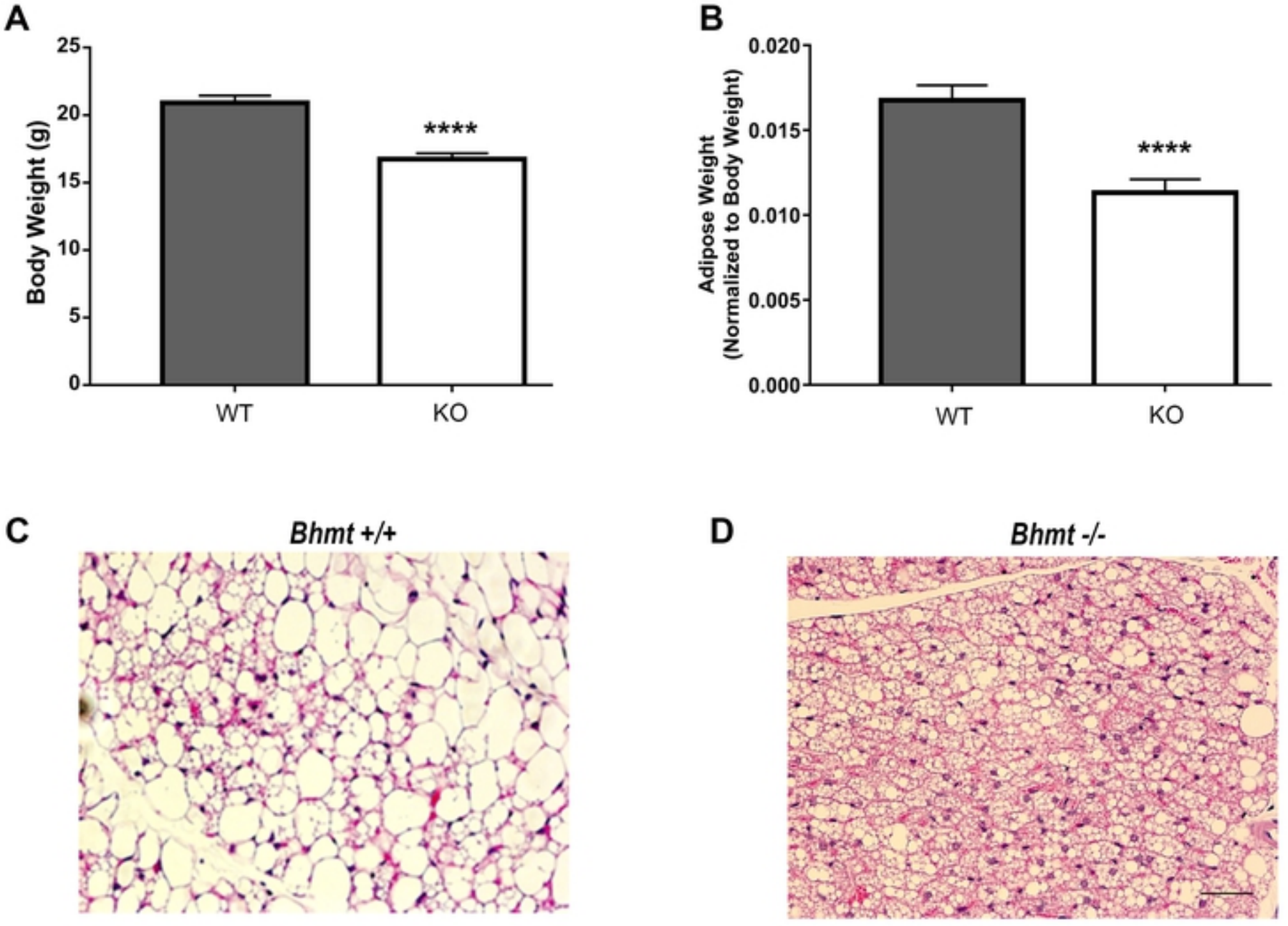

Figure 1

Figure 2

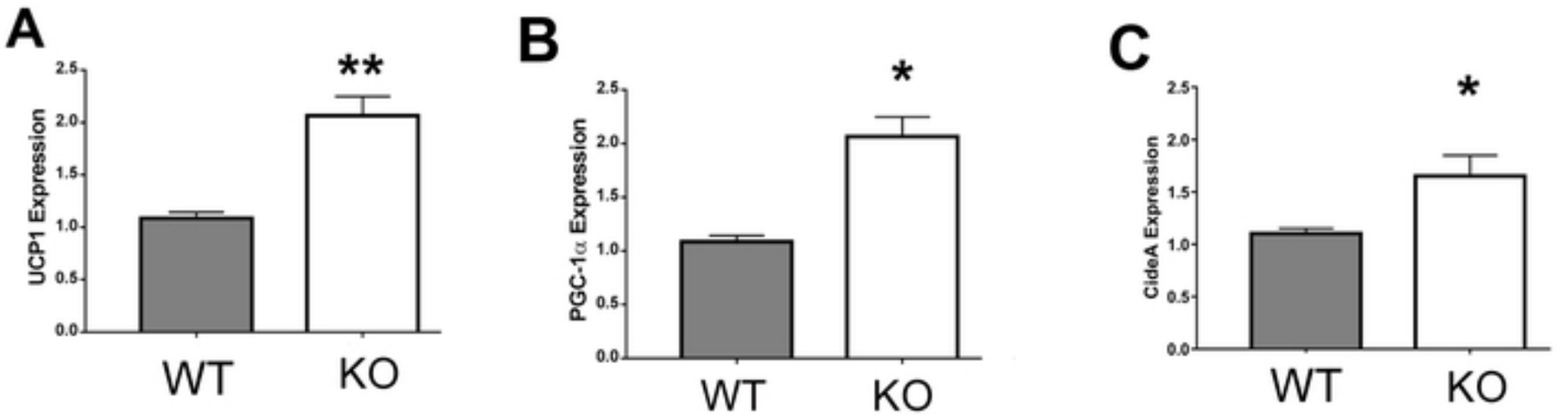

Figure 2

Figure 3

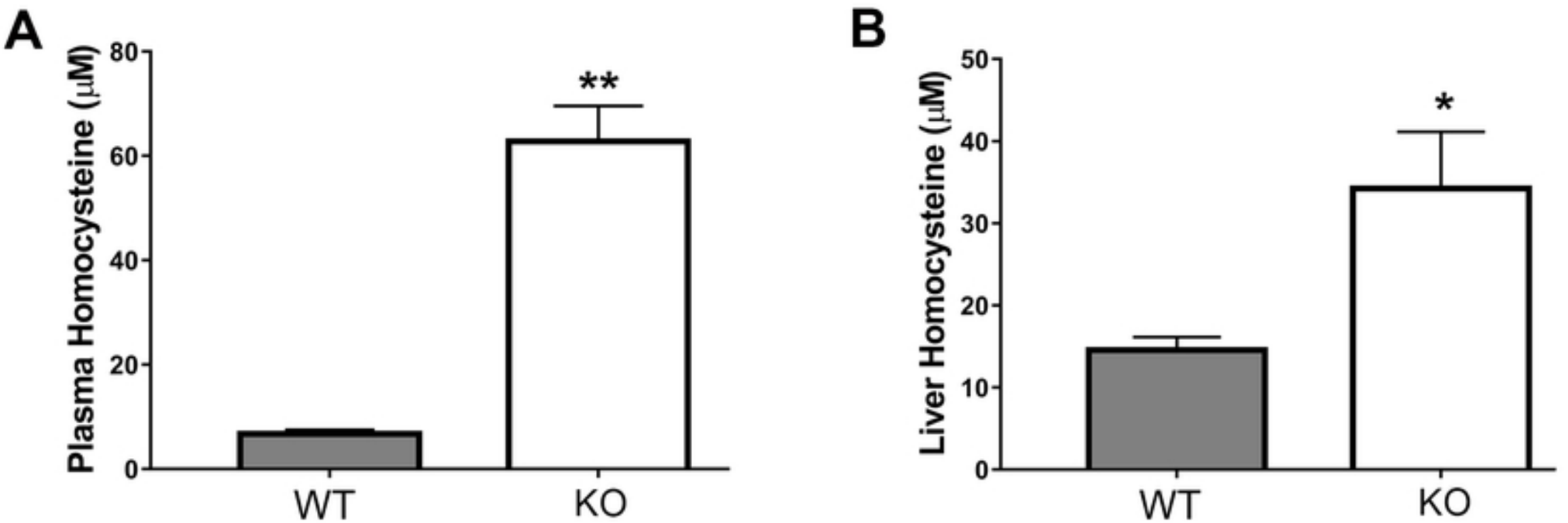

Figure 3

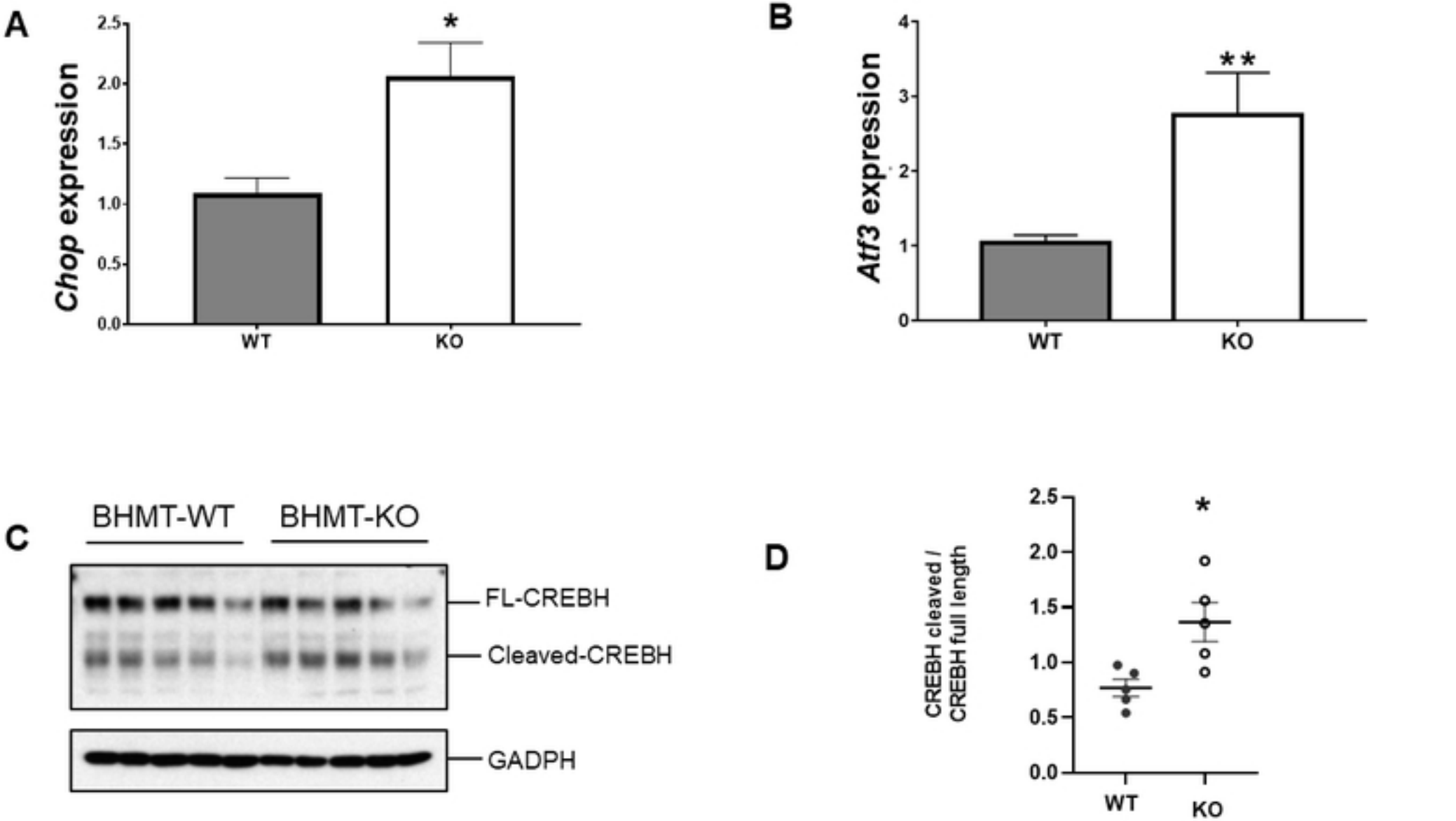
A
Chop expression
2.5
2.0
1.5
1.0
0.5
0.0
*
WT
KO
B
Atf3 expression
4
3
2
1
0
**
WT
KO
C
BHMT-WT
BHMT-KO
FL-CREBH
Cleaved-CREBH
GADPH
D
CREBH cleaved / CREBH full length
2.5
2.0
1.5
1.0
0.5
0.0
*
WT
KO

Figure 4

Figure 5

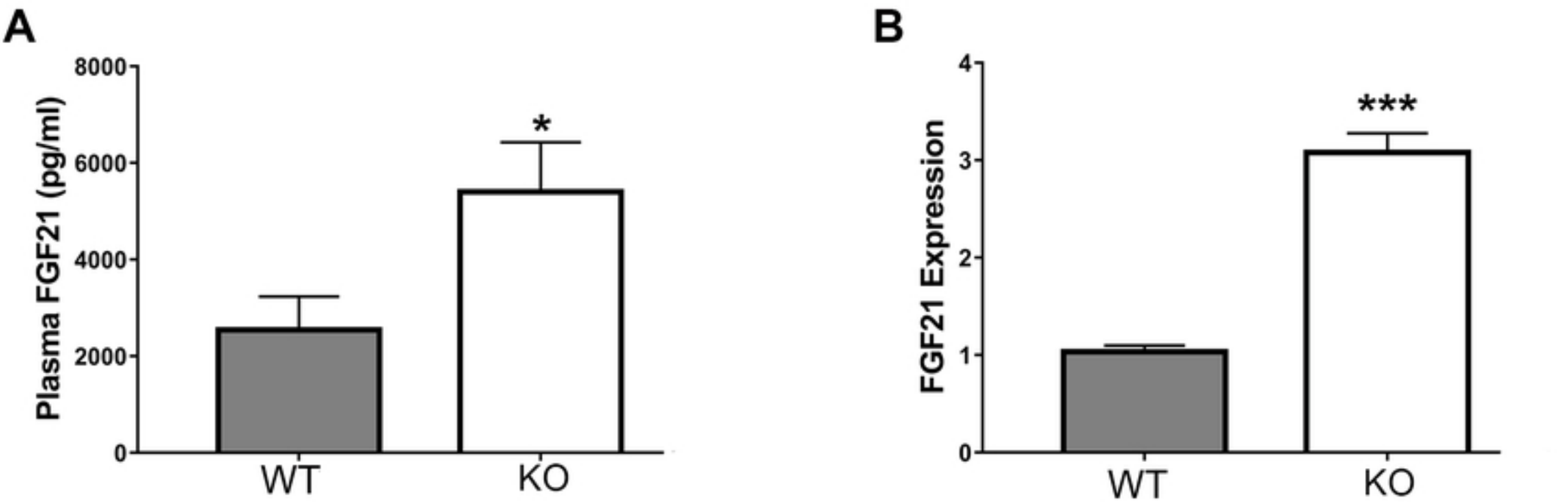

Figure 5

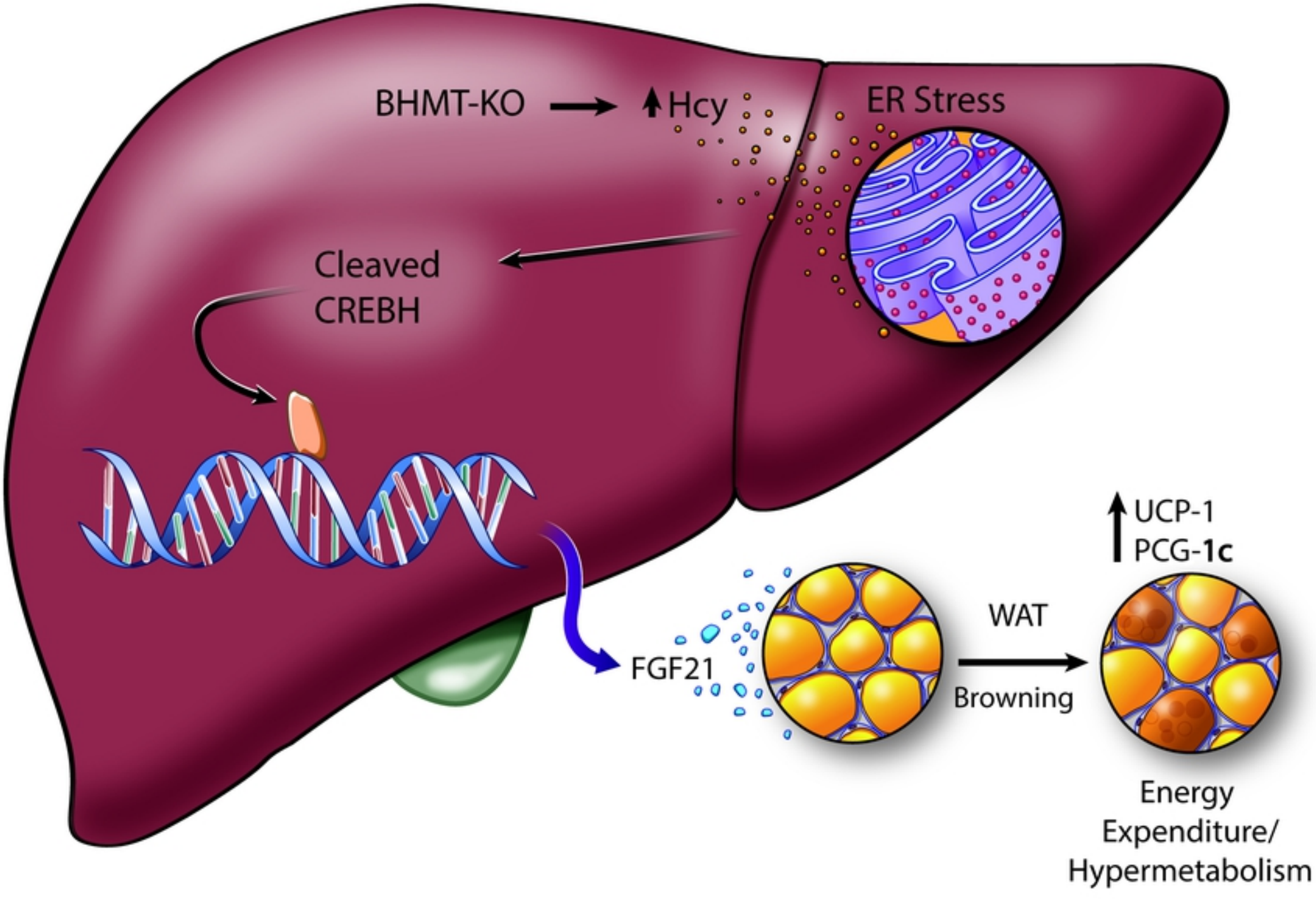
BHMT-KO
Hcy
ER Stress
Cleaved
CREBH
FGF21
WAT
Browning
UCP-1
PCG-1c
Energy
Expenditure/
Hypermetabolism

Figure 6